Static and *ab Initio* Molecular Dynamics Study of the Titanium(IV)-Constrained Geometry Catalyst ($CpSiH_2NH$)Ti-R^+. 2. Chain Termination and Long Chain Branching

Tom K. Woo, Peter M. Margl, and Tom Ziegler*

Department of Chemistry, University of Calgary, 2500 University Drive, Northwest, Calgary, Alberta, Canada T2N 1N4

Peter E. Blöchl

IBM Research Division, Säumerstrasse 4, CH-8803 Rüschlikon, Switzerland

Received February 21, 1997[⊗]

We present a comprehensive survey of chain termination and long chain branching processes for the "constrained-geometry" olefin polymerization catalyst ($CpSiH_2NH$)Ti-R^+ (R = ethyl, propyl) based on static and dynamic density functional theory. Car-Parrinello molecular dynamics calculations are used to locate reaction pathways and estimate free energies of activation, and conventional static calculations are used to ascertain stationary points and relative energies. We have examined three distinct chain termination processes: (a) β-hydrogen transfer to the monomer, (b) β-hydrogen transfer to the metal, and (c) olefin C−H σ-bond metathesis. We find alternative (a) to be the most viable one [$\Delta H^{\ddagger}_{el}$(R = ethyl) = 32 kJ/mol; $\Delta F^{\ddagger}$(R = ethyl) = 40.1; $\Delta F^{\ddagger}$(R = propyl) = 43 ± 8 kJ/mol at 300 K], whereas pathways (b) [$\Delta H^{\ddagger}_{el}$(R = propyl) = 67; $\Delta F^{\ddagger}$(R = propyl) = 57 ± 3 at 300 K] and (c) [$\Delta H^{\ddagger}_{el}$(R = ethyl) = 93; $\Delta F^{\ddagger}$(R = ethyl) = 91.7 kJ/mol; $\Delta F^{\ddagger}$(R = propyl) = 87 ± 5 at 300 K] have much higher activation barriers. In addition, we investigated an unconventional long chain branching mechanism (d), where a polymer chain binds to the metal center in an η^2-agostic fashion via aliphatic hydrogens, followed by activation of one aliphatic C−H bond and transfer of the hydrogen to the α-carbon (σ-bond metathesis). For this process we have found a large electronic barrier of $\Delta H^{\ddagger}_{el}$(R = ethyl) = 77 kJ/mol and a free energy barrier of $\Delta F^{\ddagger}$(R = ethyl) = 72.3 kJ/mol; $\Delta F^{\ddagger}$(R = propyl) = 70 ± 3 kJ/mol at 300 K. On the basis of our data, we favor the conventional long chain branching mechanism consisting of chain termination via mechanism (a) to produce a vinyl-terminated chain and reincorporation of the terminated chain into the polymer. In this study we have calculated free energy barriers for each of the aforementioned processes by a conventional static calculations and by a Car-Parrinello "first principles" molecular dynamics simulations. The agreement of the two methods is exceptional, demonstrating utility of first principles molecular dynamics to determine free energy barriers.

1. Introduction

In recent years, there have been many exciting developments in the area of metallocene and single-site catalysts for olefin polymerization. One such development is the constrained geometry catalyst (CGC) of the type ($CpSiH_2NH$)Ti-R^+ as typified in Scheme 1. It has been well-advertised[1] that CGCs produce a new family of linear polyethylenes which break the traditional rules of the structure−property−processibility relationships.[2,3] More specifically, CGCs produce polymers which possess very desirable strength properties while still allowing for favorable processibility properties. This exceptional characteristic of CGC polymers has been attributed to the inclusion of linear long chain branches into the polymer backbone, a feature not found in traditional commercial polyethylenes. CGC polymers are unique in that it is claimed that they have a *controlled* level of long chain branches. Furthermore, the long chains are linear as opposed to dendritic and are much longer than those produced by the copolymerization of traditional C_3−C_8 comonomers. In order to effect the properties of the polymer, these long chain branches are estimated to be greater than 250 carbon atoms long.[4] This type of linear long chain branching has been of commercial interest to polyethylene producers for many years, and various strategies have been developed to produce long

Scheme 1

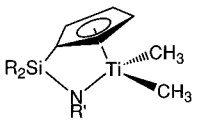

[⊗] Abstract published in *Advance ACS Abstracts,* June 15, 1997.

(1) This is most true for the constrained geometry catalyst technology commercialized by the DOW Chemical Co. under the tradename INSITE.

(2) Stevens, J. C. *Proceedings of The International Symposium on Catalyst Design for Tailor-Made Polyolefins*; Soga, K., Terano, M., Eds.; Konazawa, Japan, 1994; p 277.

(3) Chum, P. S.; Kao, C. I.; Knight, G. W. *Plast. Eng.* **1995**, June, 21.

(4) Soares, J. B. P.; Hamielec, A. E. *Macromol. Theory Simul.* **1996**, *5*, 547.

S0276-7333(97)00126-X CCC: $14.00

chain branching.[5] Constrained geometry catalysts are unique in that they offer linear long chain branching without additional comonomer, additives, or postprocessing. These unique properties of constrained geometry catalysts have accelerated their development for commercial use, and they are in fact among the first metallocene catalysts to be commercialized. In the prequel to this paper, we investigated in detail the chain propagation mechanisms pertaining to the "constrained-geometry" catalyst ($CpSiH_2NH$)Ti-R^+. In the present paper, we study several chain termination processes and we attempt to elucidate the molecular mechanism underlying the formation of long chain branched polyethylene by means of static and dynamic density functional theory. Car-Parrinello projector-augmented wave (CP-PAW) molecular dynamics calculations are used to locate reaction pathways and estimate free energies of activation, while static ADF calculations were used to ascertain stationary points and relative energies. This combination has proven fruitful already in a number of previous studies.[6−8] To our knowledge, the present paper constitutes the first successful attempt to calculate free energies of activation for bond-breaking/bond-making processes from first-principles molecular dynamics.

2. Computational Details

The reported "static" density functional calculations were all carried out by the ADF program system version 1.1.3, developed by Baerends and others.[9−12] For the description of the electronic configuration (3s, 3p, 3d, 4s, and 4p) of titanium, we used an uncontracted triple-ζ STO basis set.[13,14] For carbon (2s, 2p) and hydrogen (1s), a double-ζ STO basis, augmented with a single 3d or 2p polarization function, respectively, was applied. No polarization functions were employed for carbon and hydrogen atoms on the Cp ring. The $1s^22s^22p^63s^2$ configuration on Ti, the $1s^22s^22p^2$ configuration on Si, and the $1s^2$ shell on C and N were assigned to the core and treated with the frozen core approximation.[15] In order to fit the molecular density and to represent Coulomb and exchange potentials accurately, a set of auxiliary s, p, d, f, and g STO functions,[16] centered on all nuclei, was used in every SCF cycle. Energy differences were calculated by including the local exchange-correlation potential by Vosko[17] *et al.* with Becke's[18] nonlocal exchange corrections and Perdew's[19,20] nonlocal correlation correction. The spin-restricted formalism was used for all calculations. Geometries were optimized *without* including nonlocal corrections. In a previous publication, we have shown that in systems such as the one under investigation here the energetics derived by such a procedure deviate by less than 10 kJ/mol from energetics obtained by nonlocal geometry optimization.[21] The Becke−Perdew nonlocal density functional was recently shown to yield enthalpic barriers which are systematically smaller than the experimental free energy barriers by 13 kJ/mol on average for a Pd(II) catalyst system.[22,23] All saddle point determinations were initialized by a linear transit search from reactant to product along an assumed reaction coordinate where all degrees of freedom were optimized except for the reaction coordinate which was frozen for each step. Transition states were then fully optimized and validated by a frequency calculation where the backbone (Cp, silane, and amido groups) of the constrained-geometry catalyst was frozen. This approach was justified in ref 6. The calculation of free energies followed standard textbook procedures[24] and was based on the aforementioned constrained frequency calculations.

All reported molecular dynamics simulations were carried out with the CP-PAW code developed by Blöchl.[25] The wave function was expanded in plane waves up to an energy cutoff of 30 Ry. We employed the frozen core approximation for the [Ar] core on Ti, the [Ne] core for Si, and the [He] core of the first row elements. Periodic boundary conditions were used, with a unit cell spanned by the lattice vectors ([0.0 8.5 8.5] [8.5 0.0 8.5] [8.5 8.5 0.0]) (Å units). All simulations were performed using the local density approximation in the parametrization of Perdew and Zunger,[26] with gradient corrections due to Becke[18] and Perdew.[19,20] The accuracy of the PAW method for geometries and energetics has been established by Blöchl.[25] To prevent electrostatic interactions between neighboring unit cells, a charge isolation scheme is used.[27] To achieve an evenly distributed thermal excitation, the nuclei were brought to a temperature of 300 K by applying a sequence of 30 sinusoidal pulses, each of which was chosen to raise the temperature by 10 K. Each of the excitation vectors were chosen to be orthogonal to the already excited modes. A temperature of 300 K was maintained for all simulations by a Nosé thermostat,[28,29] which creates a canonical (NVT) ensemble. The fictitious kinetic energy of the electrons was controlled in a similar fashion by a Nosé thermostat.[30] In order to span large portions of configuration space in a minimum of time, the true masses of the nuclei were rescaled to 5.0 (Ti), 2.0 (Si, N, and C), and 1.5 (H) atomic mass units. Together with an integration time step of 7 au (∼0.17 fs), this choice ensures good energy conservation during the dynamics simulation without computational overhead due to heavy atomic nuclei. Since we do not discuss time-dependent properties and since configurational ensemble averages remain unchanged under a rescaling of the masses, this technique is appropriate. Since the nuclear velocities scale with $m^{-1/2}$ the sampling is sped up by a factor of 1.5−2. Therefore, all reported simulation times are effectively increased by a factor of 1.5−2, so that a 4 ps simulation yields a sampling accuracy corresponding to a 6 ps simulation. To sample phase space in the vicinity of the transition state, we choose a reaction coordinate (RC) which is kept constrained during the dynamics

(5) Brant, P.; Canich, J. A. M.; Dias, A. J.; Bamberger, R. L.; Licciardi, G. F.; Henrichs, P. M. International Patent Application WO 94/07930, April 14, 1994.
(6) Woo, T. K.; Margl, P. M.; Lohrenz, J. C. W.; Blöchl, P. E.; Ziegler, T. *J. Am. Chem. Soc.* **1996**, *118*, 13021.
(7) Margl, P.; Blöchl, P.; Ziegler, T. *J. Am. Chem. Soc.* **1995**, *117*, 12625.
(8) Margl, P.; Blöchl, P.; Ziegler, T. *J. Am. Chem. Soc.* **1996**, *118*, 5412.
(9) Baerends, E. J.; Ellis, D. E.; Ros, P. *Chem. Phys.* **1973**, *2*, 41.
(10) te Velde, G.; Baerends, E. J. *J. Comput. Chem.* **1992**, *99*, 84.
(11) Versluis, L.; Ziegler, T. *J. Chem. Phys.* **1988**, *88*, 322.
(12) Ravenek, W. *Algorithms and Applications on Vector and Parallel Computers*; te Riele, H. J. J., Dekker, T. J., van de Horst, H. A., Eds.; Elsevier: Amsterdam, The Netherlands, 1987.
(13) Snijders, J. G.; Baerends, E. J.; Vernoijs, P. *At. Nucl. Data Tables* **1982**, *26*, 483.
(14) Vernoijs, P.; Snijders, J. G.; Baerends, E. J. *Slater Type Basis Functions for the Whole Periodic System*; Department of Theoretical Chemistry, Free University: Amsterdam, The Netherlands, 1981.
(15) Baerends, E. J. Ph.D. Thesis, Free University, Amsterdam, The Netherlands, 1975.
(16) Krijn, J.; Baerends, E. J. *Fit Functions in the HFS Method*; Department of Theoretical Chemistry, Free University: Amsterdam, The Netherlands, 1984.
(17) Vosko, S. H.; Wilk, L.; Nusair, M. *Can. J. Phys.* **1980**, *58*, 1200.
(18) Becke, A. *Phys. Rev. A* **1988**, *38*, 3098.
(19) Perdew, J. P. *Phys. Rev. B* **1986**, *33*, 8822.
(20) Perdew, J. P. *Phys. Rev. B* **1986**, *34*, 7406.
(21) Lohrenz, J. C. W.; Woo, T. K.; Ziegler, T. *J. Am. Chem. Soc.* **1995**, *117*, 12793.
(22) Margl, P. M.; Ziegler, T. *J. Am. Chem. Soc.* **1996**, *118*, 7337.
(23) Margl, P. M.; Ziegler, T. *Organometallics* **1996**, *15*, 5519.
(24) McQuarrie, D. A. *Statistical Thermodynamics*; Harper & Row: New York, 1973.
(25) Blöchl, P. E. *Phys. Rev. B* **1994**, *50*, 17953.
(26) Perdew, J. P.; Zunger, A. *Phys. Rev. B* **1981**, *23*, 5048.
(27) Blöchl, P. E. *J. Chem. Phys.* **1995**, *103*, 7422.
(28) Hoover, W. G. *Phys. Rev. A* **1985**, *31*, 1695.
(29) Nosé, S. *Mol. Phys.* **1984**, *52*, 255.
(30) Blöchl, P. E.; Parrinello, M. *Phys. Rev. B* **1992**, *45*, 9413.

Scheme 2

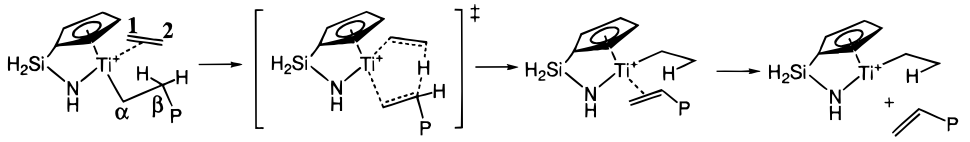

Scheme 3

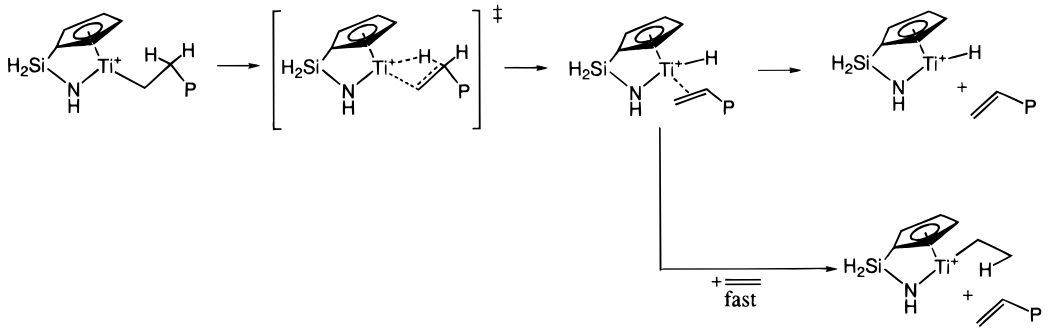

Scheme 4

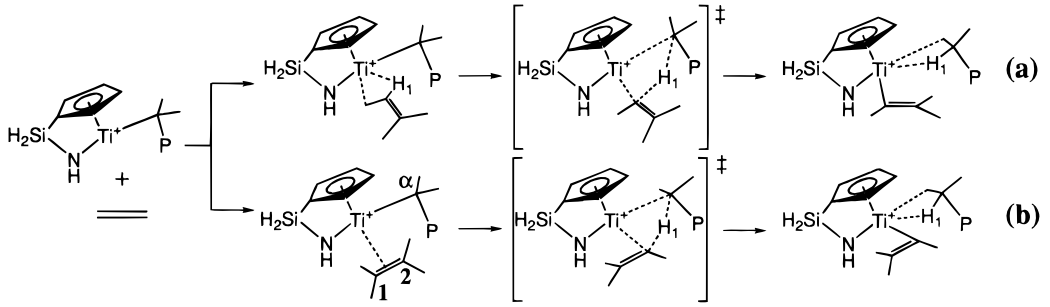

using SHAKE[31] constraints. It is desirable that the RC has a high projection onto the IRC[32] (intrinsic reaction coordinate). All other degrees of freedom are allowed to evolve naturally in time. By slowly varying the constraint, phase space in the vicinity of the transition state can be sampled dynamically, leading to undisturbed dynamics for all motions which are orthogonal to the RC and to fictitious dynamics along the RC. This "slow-growth" technique allows us to investigate even high-lying transition states. The total scan time chosen was about 35 000 time steps (~6 ps real time) for slow-growth simulations. The free energy difference ΔF between two arbitrary points $\lambda = 0$ and $\lambda = 1$ along the reaction coordinate was determined as

$$\Delta F = \int_0^1 \langle \partial E/\partial\lambda \rangle|_{\lambda,T}\, \mathrm{d}\lambda \qquad (1)$$

where λ is just a linear parameter representing any path connecting the two points and the integrand is the appropriately scaled averaged force on the RC sampled at constant temperature and λ. ΔF as derived by this formula does not rely on the harmonic approximation that would be used in the standard treatment based on second derivatives of the total energy. Note that it does not include quantum effects. Thus, in order to more formally compare ΔF as determined from the slow-growth molecular dynamics simulation, the zero-point energy and ΔH_{vib}[33] must not be included in the ΔF obtained from the static frequency calculation. For eq 1 to give correct results, $\langle \delta E/\delta\lambda \rangle$ must be determined at a large number of λ points between 0 and 1. Furthermore, for each λ point an extensive sampling is required at constant T to determine the proper average $\langle \delta E/\delta\lambda \rangle_{\lambda,T}$. In the slow-growth limit, λ is scanned continuously so that only a single value of $\delta E/\delta\lambda$ is determined at each value of λ. This method has the advantage of not disrupting the dynamics when the value of λ is changed. The slow-growth method has been previously demonstrated on several elementary reaction steps in organometallic chemistry.[6−8,34] It should be noted that both the static and dynamic simulations are at the zero pressure limit.

3. Results and Discussion

3.a. Chain Termination. Chain termination plays a critical role in determining the fundamental property of polymer molecular weight. With constrained geometry catalysts, chain termination may play an additional role in long chain branching since the favored mechanism for the branching involves the reinsertion of vinyl-terminated chains.[3] We have examined three distinct chain termination processes: (a) β-hydrogen transfer to the monomer, (b) β-hydrogen transfer to the metal (often referred to as β-hydride elimination), and (c) monomer C−H σ-bond metathesis. These three chain termination processes are shown in Schemes 2, 3, and 4, respectively.

***β*-Hydrogen Transfer to the Monomer.** Bimolecular β-hydrogen transfer to the monomer (Scheme 2) has been studied theoretically for bis-Cp metallocenes.[34−37] These studies suggest that β-hydrogen transfer to the

(31) Ryckaert, J.-P.; Ciccotti, G.; Berendsen, H. J. C. *J. Comput. Phys.* **1977**, *23*, 327.
(32) Fukui, K. *Acc. Chem. Res.* **1981**, *14*, 363.
(33) Since the classical vibrational energy levels are continuous, $H_{\mathrm{vib}} = \sum RT/2$ for both reactants and transition states. Therefore $\Delta H^{\ddagger}_{\mathrm{vib}} = 0$ for the MD simulations.
(34) Margl, P.; Lohrenz, J. C. W.; Blöchl, P.; Ziegler, T. *J. Am. Chem. Soc.* **1996**, *118*, 4434.
(35) Lohrenz, J. C. W.; Woo, T. K.; Fan, L.; Ziegler, T. *J. Organomet. Chem.* **1995**, *497*, 91.
(36) Cavallo, L.; Guerra, G. *Macromolecules* **1996**, *29*, 2729.

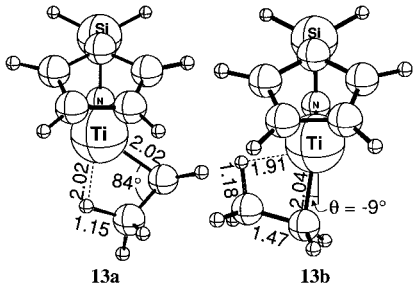

Figure 1. Optimized Ti−ethyl cation structures. Relevant bond distances are reported in angstroms and angles in degrees. The parameter θ in **13b** is the angle between the Ti−C_α bond vector and the meridional Ti−N−Cp centroid plane.[6]

monomer is the preferred chain termination mechanism for zirconocenes with an electronic barrier of $\Delta H^{\ddagger}_{el}$ = 28 kJ/mol. For the CGC system we have examined this termination process with both conventional static methods and the CP-MD method. In the static calculations, an ethyl group was used as the model for the growing chain whereas a larger propyl model was used for the CP-MD simulation.

For the static simulations, two channels were explored, one commencing from the π-complex **10b** and the other from the planar π-complex **10d**. (Structures **10b** and **10d** are shown in Figure 9 of ref 6.) Note that we preserve and continue the numbering of species introduced in the prequel to this work[6] to avoid ambiguities. The lowest energy channel was found to originate from the planar π-complex **10d**. For completeness we have included the isomerization barrier from **10b** to **10d** which has already been discussed in relation to the insertion process.[6] The results of the conventional static calculations are shown in Figure 2, where the energy of the preferred π-complex (as established in ref 6) **10b** has been used as a baseline.

The transition state, **12**‡, related to transfer of hydrogen through this channel, is shown in Figure 3 and lies 31.7 kJ/mol above **10b**. The calculated free energy barrier based on a frequency calculation was determined to be $\Delta F^{\ddagger}$ = 40.1 kJ/mol. The initial product of the process is another β-agostic π-complex where the vinyl-terminated growing chain is π-coordinated to the metal. In our model system, this product is equivalent to **10d** except for a mirror symmetry operation. Figure 2a also details the energetics required to fully remove the vinyl-terminated chain from the Ti−ethyl cation to form free ($CpSiH_2NH$)Ti−ethyl$^+$, **13a** (Figure 1), plus free ethene. For our model system the process is endothermic by 72.9 kJ/mol. In solution, full dissociation of the vinyl-terminated polymer chain is likely to involve substitution with either monomer or solvent which is significantly less endothermic.[38]

In addition to the H-transfer channel initiated from the planar π-complex **10d**, we also examined the H-transfer channel proceeding from the preferred frontside π-complex **10b**. This channel (not shown) resulted in a slightly higher reaction barrier of $\Delta H^{\ddagger}_{el}$ = 36.1 kJ/mol. Since the number of possible reaction channels is obviously quite large given the number of possible initial

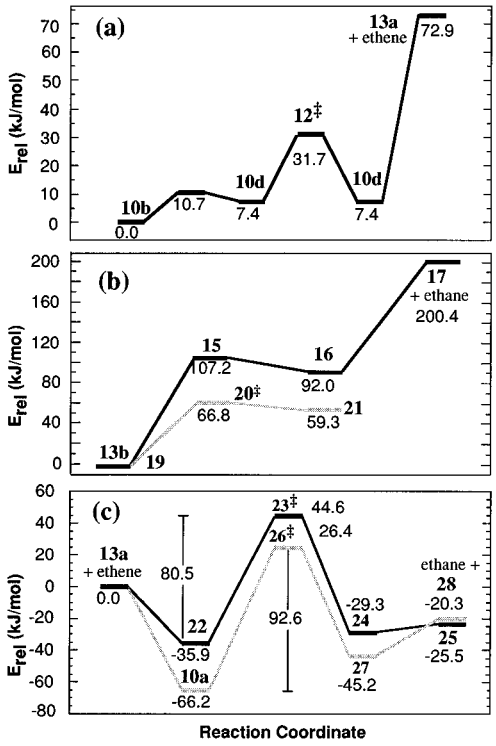

Figure 2. Static chain termination profiles (ΔH_{el}): (a) Hydrogen transfer to the monomer. (b) Hydrogen transfer to the metal. The solid profile represents the elimination profile when the growing chain is modeled with an ethyl group whereas the shaded profile depicts the process when a propyl group is used to model the growing chain. (c) Monomer (olefin) σ-bond metathesis. Solid profile represents end-on channel a and the shaded profile represents channel b. Refer to Scheme 4.

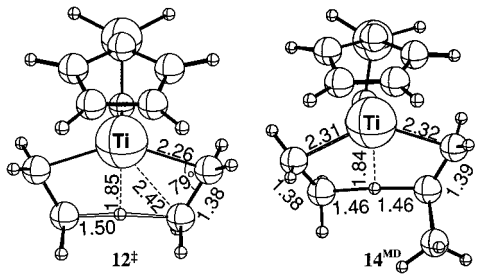

Figure 3. Hydrogen transfer to monomer transition state structures. **12**‡ is the optimized transition state structure from the conventional static calculation. Structure **14**^{MD} is an arbitrary snapshot from the CP-MD simulation at a midplane RC value of 0.5. Bond distances are in angstroms and angles are presented in degrees.

and final configurations, we have employed the CP-MD method to more efficiently sample the available phase space during the transfer process.

A CP-MD simulation of the β-hydrogen transfer to the monomer was performed, with a propyl group serving as a model of the growing chain. A unique slow-growth reaction coordinate (RC) that is detailed in Figure 4 was utilized in the simulation. This reaction coordinate is defined as the ratio r/R where R is the length of the vector between C_2 and C_β (see Scheme 2 for labeling) and r is the length of projection of the C_β−H_β bond vector onto the vector **R**. This reaction coordinate constrains the transferring H atom to lie on the plane perpendicular to and passing through the endpoint of the vector **r**.

(37) Fan, L.; Harrison, D.; Deng, L.; Woo, T. K.; Swerhone, D.; Ziegler, T. *Can. J. Chem.* **1995**, *73*, 989.

(38) A similar process is shown in Scheme 3b with respect to the β-hydrogen transfer to the metal.

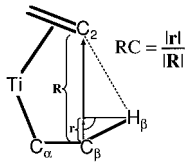

Figure 4. The midplane slow-growth reaction coordinate definition for the hydrogen transfer to monomer reaction (Scheme 2).

Commencing the simulation from the β-agostic π-complex, the value of the RC is initially small (approximately 0.25), indicating that the H atom to be transferred is still bound to the C_β of the alkyl chain. As the reaction progresses, the length of the vector **r** is steadily increased until at the approximate transition state the RC is 0.5, indicating that the H_β lies on a plane midway between the two atoms C_β and C_2. For lack of a better label, we have termed this reaction coordinate the midplane constraint. The midplane constraint was used because it is presumed to be the most reversible reaction coordinate for the transfer process and therefore the least susceptible to large hysteresis.[39]

We have performed a bidirectional scan of the H-transfer process from the β-agostic π-complex to the approximate transition state.[40] We have focused our computational effort to simulate the first half of the transfer process from the reactant to the transition state, and not from the transition state to the product, since we are principally interested in the determination of the free energy barrier for the process. Figure 5b traces the C_2-H_β, $C_\beta-H_\beta$, and $Ti-H_\beta$ distances as a function of the midplane reaction coordinate for the forward scan. Since there are no notable differences in the geometrical parameters for the forward and reverse scans, only the results of the forward scan are presented in parts b and c Figure5. At the transition state when the RC is 0.5, the C_2-H_β and $C_\beta-H_\beta$ distances converge to a value of roughly 1.5 Å, consistent with the static transition state structure **12**‡. Structure **14**$^{\mathbf{MD}}$, shown in Figure 3, is a snapshot of the system at a reaction coordinate value of 0.50. All structures taken from the Car-Parrinello simulations are appended with the MD superscript in order to emphasize that they are arbitrary snap shots taken from a specified portion of the molecular dynamics trajectory and not stationary points. The transfer process which is stabilized by a $Ti-H_\beta$ interaction shows that the $Ti-H_\beta$ distance converges to a distance of roughly 1.9 Å, again in good agreement with the static calculations. The $C_1-C_2-C_\beta-C_\alpha$ dihedral angle plotted in Figure 5c demonstrates the planarity of the olefin moiety and the $C_\alpha-C_\beta$ atoms of the propyl chain. Initially there are large fluctuations in the dihedral due to the free rotation of the olefin about the Ti−olefin midpoint axis; however, as the reaction progresses to the transition state, the fluctuations decrease. Additionally, the value of the $C_1-C_2-C_\beta-C_\alpha$ dihedral does not converge to 0°, but rather to a value of approximately 20°. This shows that the transition state for a propyl chain is not strictly planar but

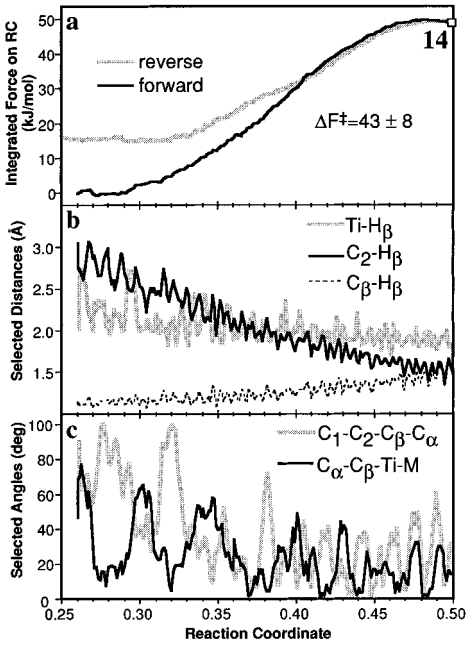

Figure 5. Selected structural and energetic quantities as a function of the reaction coordinate from the Car-Parrinello molecular dynamics simulation of the hydrogen transfer to monomer reaction (Scheme 2):[40] (a) the integrated force on the reaction coordinate for both the forward and reverse scan and (b) selected distances and (c) selected dihedral angles for the forward scan. The midplane constraint defined in Figure 4 was used as the slow growth reaction coordinate. The initial value of 0.26 approximates a β-agostic π-complex and the final value of 0.5 approximates the transition state.

slightly twisted, in contrast to the nearly planar transition state of the static calculations, **12**‡, in which the H atom is transferred from an ethyl group. It is possible therefore that there are notable differences in the transition state for the transfer process when the growing chain is modeled with groups larger than ethyl. However, we have not explored this with further static calculations.

The integrated force on the reaction coordinate is plotted in Figure 5a for both the forward and reverse directions of the bidirectional scan. The forward process (from reactant to transition state) gives a free energy barrier of approximately 50 kJ/mol, whereas the reverse process (from transition state to reactant) produces a free energy barrier of approximately 35 kJ/mol. Analysis of both forward and reverse trajectories reveals that the same transfer channel is followed in both the forward and reverse direction and the energy differences are due to a systematic bias caused by the scan velocity. The average barrier of the forward and reverse process is 43 kJ/mol, with an error bar of ±8 kJ/mol. Given that a different model served as the growing chain, this is in remarkable agreement with the static calculation which provides a free energy barrier of $\Delta F^{\ddagger}$(R = ethyl) = 40.1 kJ/mol.[41] The difference of +11 kJ/mol to the static $\Delta H^{\ddagger}_{el}$ result indicates that there is an unfavorable

(39) Hysteresis refers to the difference in sampling between forward and reverse scans of the same process. A similar effect is sometimes observed with static linear transit calculations where forward and backward scans do not provide the same picture.

(40) Animations of all the presented molecular dynamics simulations (forward scans) can be found at our research group's world wide web home page at <http://www.chem.ucalgary.ca/groups/ziegler>.

(41) It should be noted that the free energy barrier from the static simulation as determined from a frequency calculation also includes the zero-point energy correction and ΔH_{vib} whereas the dynamical estimate does not include these since the dynamics is classical. If the zero point energy correction and ΔH_{vib} are not included, the free energy barrier obtained from the static calculations is 43.0 kJ/mol. Further details are discussed in Section 4.

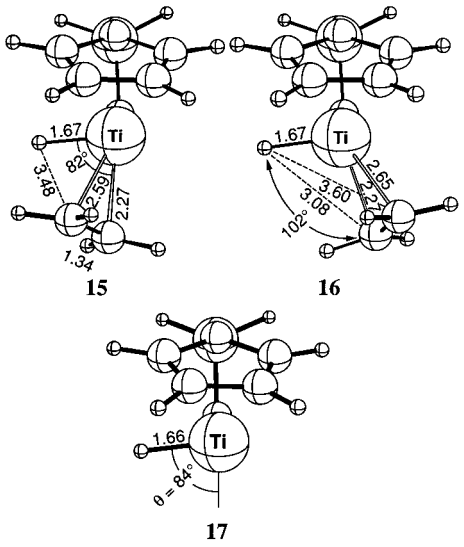

Figure 6. Optimized static structures related to the hydrogen transfer to the metal (β-hydride elimination) process (Scheme 3) whereby the growing chain is modeled by a ethyl chain. **15** is an approximate transition state due to a linear transit calculation, **16** is the optimized hydride olefin intermediate, and **17** is the Ti−hydride cation. Distances are reported in angstroms and angles in degrees.

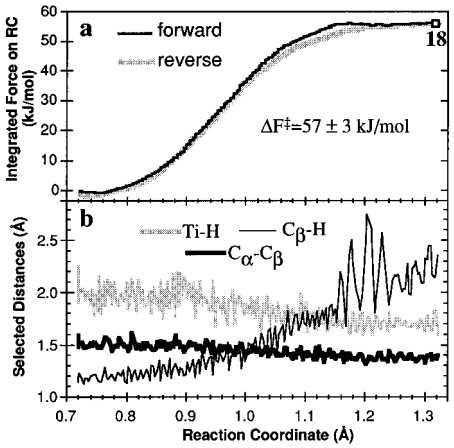

Figure 7. Selected structural and energetic quantities as a function of the reaction coordinate from the Car-Parrinello molecular dynamics simulation of the hydrogen transfer to metal reaction (Scheme 3).[40] (a) The integrated force on the reaction coordinate for both the forward and reverse scan. (b) Selected distances for the forward scan only. The reaction coordinate utilized is the distance from C_β to the center of mass of the two H_β atoms. The initial value of 0.7 corresponds to the β-agostic Ti−propyl cation. The relative free energy of the snapshot structure **18**^{MD} (Figure 8) is shown in (a).

entropic contribution involved in the formation of the more "constrained" transition state.

***β*-Hydrogen Transfer to the Metal.** Unimolecular β-hydride transfer to the metal or β-hydride elimination as shown in Scheme 3 has been previously studied theoretically[21,36,42−44] for bis-Cp metallocenes. These studies suggest that the process is not competitive with other termination processes, in particular H-transfer to monomer. However, this is an area of debate since there is experimental evidence which both favors and disfavors β-hydrogen transfer to the monomer as the preferred termination mechanism.[45] We have explored β-hydride transfer to the metal for the constrained geometry catalyst with static and dynamic calculations.

The energy profile resulting from the static calculation is shown as the solid profile in Figure 2b, and relevant structures are shown in Figure 6. Again, an ethyl group is used as the model for the growing alkyl chain such that P = H in Scheme 3. In this calculation, a hydride π-olefin complex **16** was first optimized. A linear transit calculation revealed that as the $H_\beta-C_\beta$ distance was contracted from its initial value in **16**, the backside[46] β-agostic Ti−ethyl complex **13b** (Figure 1) was formed. The Ti−ethyl$^+$ complex **13b** is analogous the Ti−butyl$^+$ structure **3d** of part I of this study.[6] The energies presented in Figure 6 are therefore relative to **13b**.

Figure 2b shows that there is a 107.2 kJ/mol electronic barrier to the formation of the hydride−olefin complex. The hydride−olefin complex **16** itself is greatly destabilized, lying 92.0 kJ/mol higher than the β-agostic Ti−ethyl complex. Further dissociation of the olefin to form the uncoordinated hydride, **17**, and free olefin is endothermic by an additional 108.4 kJ/mol. The overall process from the β-agostic alkyl complex, **13b**, to the uncoordinated hydride, **17**, and free olefin is endothermic by 200.4 kJ/mol. The high barriers and endothermicities of the process are consistent with calculations on similar bis-Cp titanocenes and zirconocenes.[35,36,43,44]

To locate the hydride elimination path for the analogous propyl system, we performed a bidirectional PAW slow-growth simulation, using the distance between C_β and the center of mass of the two β-hydrogen atoms as the reaction coordinate in order not to bias the reaction toward a particular hydrogen atom and in order to achieve reversibility. Figure 7b tracks several distances as a function of the reaction coordinate for the forward scan. Here the reaction coordinate has a value of 0.72 Å in the initial β-agostic Ti−propyl cation and a value of 1.32 Å in the olefin−hydride complex. The thin solid line traces the $H-C_\beta$ distance which gradually expands, as expected, during the course of the simulation. The bold solid line follows the $C_\alpha-C_\beta$ distance which slowly decreases from an initial value of approximately 1.5 Å to roughly 1.35 Å as the olefinic nature of the bond develops. The shaded line depicts the $H_\beta-Ti$ distance which slowly decreases from an agostic bonding distance of 2 Å to a distance of roughly 1.7 Å characteristic of the hydride complex. A snapshot structure, **18**^{MD}, of the hydride−olefin complex from the MD simulation at a reaction coordinate value of 1.32 Å is shown in Figure 8.

Dilation of the RC results in a steady increase of the relative free energy, as shown in Figure 7a, until a plateau is reached at RC ≈ 1.2 Å. No minimum could be located for an olefin−hydride complex from the average of the integrated forces of both scan directions. Thus, the MD results suggest that at room temperature an olefin hydride does not exist. The free energy difference between the plateau level and the ground state was found to be 57 kJ/mol, with a very small error

(42) Sini, G.; Macgregor, S. A.; Eisenstein, O.; Teuben, J. H. *Organometallics* **1994**, *13*, 1049.
(43) Woo, T. K.; Fan, L.; Ziegler, T. *Organometallics* **1994**, *13*, 2252.
(44) Yoshida, T.; Koga, N.; Morokuma, K. *Organometallics* **1995**, *14*, 746.
(45) Brintzinger, H. H.; Fischer, D.; Mülhaupt, R.; Rieger, B.; Waymouth, R. M. *Angew. Chem., Int. Ed. Engl.* **1995**, *34*, 1143.
(46) The "backside" and "frontside" terminology is detailed in part 1 of this study.[6]

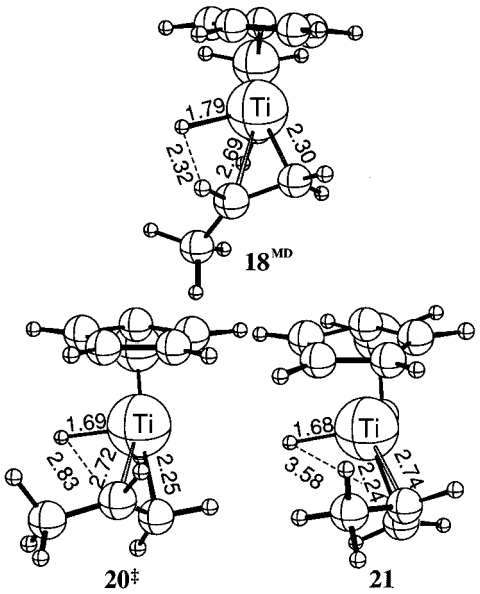

Figure 8. Structures related to the hydrogen transfer to the metal (β-hydride elimination) process (Scheme 3) whereby the growing chain is modeled by a propyl chain. **18^{MD}** is a snapshot structure from the MD simulation at a RC value of 1.32 Å representing a hydride−olefin-like complex. **20‡** is the optimized transition state from the static calculations, and **21** is the optimized Ti−hydride−olefin complex.

bar of ±3 kJ/mol. This is in striking contrast to the result of the static calculations, which yielded an ethalpic barrier of 107.2 kJ/mol for the abstraction of hydride from the ethyl group. This large discrepancy was thought to be due to the different models for the growing alkyl chain. A similar effect has been found by Bercaw and co-workers[47] who have observed for Cp_2*Sc-R there is an increased rate of β-elimination for R = propyl as compared to R = ethyl. To validate that this may also be true for the present system, static calculations were performed whereby the growing chain was modeled by a propyl group.

The shaded profile in Figure 2b depicts the elimination profile with a propyl growing chain. In agreement with the CP-MD simulation, the process is much less endothermic when growing chain is modeled with a propyl group as compared to when it is modeled with an ethyl group. We find that the hydride−olefin complex **21** lies 59.3 kJ/mol above the initial β-agostic Ti−propyl cation. We have located a transition state **20‡** for the process which lies 66.8 kJ/mol above the initial Ti−propyl structure and only 7.5 kJ/mol above the hydride−olefin complex **21**. At 300 K, the calculated free energies of the transition state, **20‡**, and the hydride−olefin complex, **21**, are 53.9 and 47.6 kJ/mol, respectively. This result is in good agreement with the CP-MD estimate of the free energy barrier of $\Delta F^{‡} = 57 \pm 3$ kJ/mol and the fact that the hydride−olefin complex is relatively unstable.

The large discrepancy in the stability of the Ti−hydride π-olefin complexes and also the β-hydride elimination barriers when the growing chain is modeled by an ethyl group (R = H) as compared to a propyl group (R = methyl) can be rationalized in terms of electronic

Scheme 5

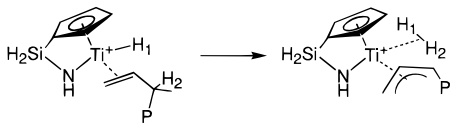

effects and in terms of the energy required to homolytically cleave the C−H bond in a secondary carbon compared to that in a primary carbon. Bercaw and coworkers[47] have addressed this for similar scandocene systems were it was observed that substitution of a hydrogen at the β-carbon by a methyl group resulted in an increase in the β-elimination rate. Here it was argued that alkyl groups are inductively electron donating with respect to hydrogen and therefore stabilize the hydride and transition state. It was further argued that the resting state metal−alkyl complex is more stable for Cp^*_2Sc−ethyl system as compared to the Cp^*_2Sc−propyl system due to steric factors. (This has the effect of increasing the elimination barrier for ethyl compared to propyl.) We have performed an energy decomposition analysis[48,49] to verify these assertions for the Ti CGC systems. Our analysis[50] reveals that the C_β−H bond in the Ti−ethyl complex is stronger than that in the Ti−propyl complex. We have also found that the methyl group enhances the stability of the hydride π-complex and therefore also the transition state. However, we also find that for the Ti CGC system the methyl group does not destabilize the Ti−propyl complex relative to the Ti−ethyl complex, but rather provides stabilization in the Ti−propyl complex. This stabilization, however, is significantly less than the stabilization found in the transition state and hydride. We conclude that the ethyl moiety is not an appropriate group to model the growing chain to simulate the β-hydride elimination process. Therefore the calculated β-hydride elimination barriers in our earlier papers[21,36,43] are expected to be over estimated.

We have found from both static and dynamic simulations that the hydride−olefin (**18^{MD}** and **21**) complex can readily isomerize into a allyl−dihydrogen complex[51] as sketched in Scheme 5. The allyl complex was found to be 37 kJ/mol more stable than the hydride−olefin complex. The details of these simulations will be presented in a future paper.[52]

Olefin σ-Bond Metathesis. In conventional bis-Cp metallocene-based olefin polymerization systems, experimental evidence indicates that chain termination is dominated by a β-hydrogen[53] transfer processes,

(47) Burger, B. J.; Thompson, M. E.; Cotter, W. D.; Bercaw, J. E. *J. Am. Chem. Soc.* **1990**, *112*, 1566.

(48) Ziegler, T. In *Metal-Ligand Interactions: From Atoms, to Clusters, to Surfaces*; Salahub, D. R., Russo, N., Eds.; Kluwer Academic Publishers: Durdrecht, 1992; Vol. NATO ASI C 378, pp 367.

(49) Ziegler, T.; Rauk, A. *Theor. Chim. Acta* **1977**, *46*, 1.

(50) To determine the extra stability incurred by the additional methyl group in **21** as compared to **16**, we have decomposed the following reactions: (i) $(CpSiH_2NH)Ti\text{-}CH_2CH_2R^+ \rightarrow (CpSiH_2NH)Ti^{\bullet+} + {}^{\bullet}CH_2CH_2R$, ΔH = 370.3 (R = H) and 376 kJ/mol (R = CH_3). (ii) $(CpSiH_2NH)Ti^{\bullet+}$ + ${}^{\bullet}CH_2CH_2R$ (geometry of Ti−alkyl complex) → $(CpSiH_2NH)Ti^{\bullet+} + CH_2{=}CH_2R\cdots H^{\bullet}$ (geometry of hydride−olefin complex) ΔH = 189 kJ/mol (R = H) and 175 kJ/mol (R = CH_3). (iii) $(CpSiH_2NH)Ti^{\bullet+} + CH_2{=}CH_2R\cdots H^{\bullet} \rightarrow (CpSiH_2NH)Ti^{+}HCH_2{=}CH_2R$, ΔH = −470 kJ/mol (R = H) and −492 kJ/mol (R = CH_3).

(51) Relevant geometric parameters from the optimized geometry of the allyl-dihydrogen complex are as follows: H−H distance = 0.83 Å; Ti−H distances = 1.87, 1.87 Å; and C−C distances = 1.38, 1.40 Å.

(52) Woo, T. K.; Margl, P. M.; Blöchl, P. E.; Ziegler, T. Work in progress.

(53) In the case of α-olefin polymerization or copolymerization, β-methyl transfer to the metal is included here.

whereas termination by olefin σ-bond metathesis is believed to be a minor process.[45] However in the case of the $[Cp^*SiNR)Sc]_2(\mu\text{-}CH_2CH_2CH_2CH_3)_2$ constrained-geometry catalyst, Bercaw and co-workers found no evidence (presence of vinylic chain ends) of β-hydrogen transfer in the polypropylene that is produced.[54] Thus, olefin σ-bond metathesis was cited as a potentially important termination process in these systems. Our calculations of bis-Cp metallocenes[55] indicate that olefin σ-bond metathesis has a modest barrier and is electronically feasible in such systems. It was therefore felt that an examination of this termination mechanism would be valuable.

Scheme 4 displays the general process through two distinct channels, a and b. With both channels there is first a complexation of the olefin. In channel a, the olefin forms an "end-on" adduct with the Ti center whereas with channel b the olefin coordinates to the metal in the familiar π-fashion. In both channels the system passes through a four-centered transition state where the olefinic H atom is transferred to the α-carbon of the alkyl chain in a σ-bond metathesis reaction. The initial product of both channels is a Ti−vinyl cation which is coordinated to the terminated alkyl chain.[56] Both olefin σ-bond metathesis channels a and b (Scheme 4) have been studied with traditional static methods where the growing chain has been approximated with an ethyl group. The calculated energy profiles are shown in Figure 2c (channel a, solid; channel b, shaded), and the optimized stationary point structures are displayed in Figure 9a,b.

The solid reaction profile in Figure 2c represents the end-on pathway, channel a. The formation of the end-on olefin adduct **22** which is shown in Figure 9a was found to be exothermic by 35.9 kJ/mol. Compared to π-coordination, which yields approximately 70 kJ/mol, the end-on coordination of the olefin is only half as favorable in this respect. Initial attempts[57] to optimize the end-on olefin complex, **22**, resulted in the formation of a π-complex, revealing that the end-on complex is only weakly stable. The transition state of channel a (**23**‡) lies 44.6 kJ/mol above the free reactants, giving rise to an electronic barrier of 80.5 kJ/mol for the process. Further transfer of the H atom leads to the formation of a Ti−vinyl−ethane adduct, **24**, which is 29.3 kJ/mol more stable than the free reactants. The products of the process, the free ethane molecule and the free Ti−vinyl complex, **25**, lie −25.5 kJ/mol below the free reactants.

Reaction channel b, which commences with the formation of a π-complex as opposed to the end-on olefin complex, **22**, is shown as the shaded reaction profile in Figure 2c. Channel b was initiated from the rotated π-complex **10a**, as opposed to the more stable π-complex

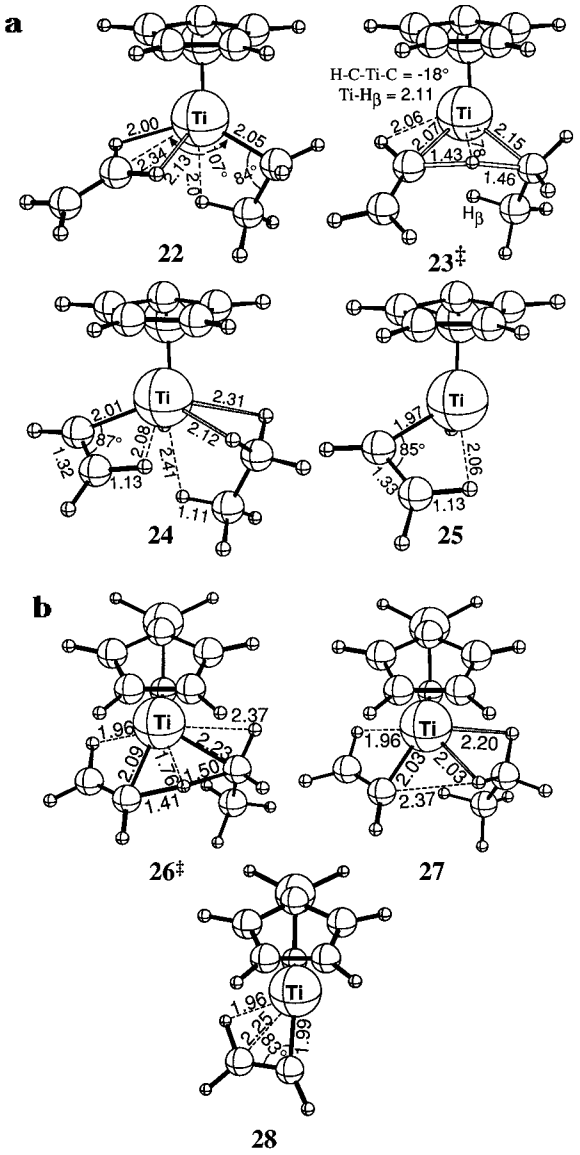

Figure 9. Optimized structures related to the olefin σ-bond metathesis chain termination process: (a) reaction channel a, (b) reaction channel b (see Scheme 4 and Figure 2c).

10b since the β-agostic H atom in **10a** does not reside on the reaction plane, thus allowing for the metathesis to occur. This is reasonable considering the static and dynamic results of the insertion process.[6]

In channel b, as the H-transfer takes place the π-coordinated olefin rotates about its double bond axis such that the angle between the Ti−olefin midpoint vector and the plane of the olefin decreases. The Ti−C_2−C_1−H_1 dihedral angle can be used to measure this rotation. In the π-complex, this angle is nearly 90°, characteristic of π-coordination of the olefin, and in the transition state, this dihedral is nearly 0°, characteristic of an edge on orientation of the olefin. The rotation of the complexed olefin occurs in concert with the transfer of the H atom since no edge-on olefin intermediate akin to **22** was located. The transition state, **26**‡, was located 26.4 kJ/mol above the free reactants and 92.6 kJ/mol above the π-complex **3b**. The transition state of channel b lies 18.2 kJ/mol below its counterpart of channel a. The resulting Ti−vinyl−ethane adduct, **27**, is 45.2 kJ/mol more stable than the free reactants and 15.9 kJ/mol more stable than the same adduct of channel a. The

(54) Shapiro, P. J.; Cotter, W. D.; Schaefer, W. P.; Labinger, J. A.; Bercaw, J. E. *J. Am. Chem. Soc.* **1994**, *116*, 4623.

(55) Ziegler, T.; Folga, E.; Berces, A. *J. Am. Chem. Soc.* **1993**, *115*, 636.

(56) Full dissociation of the resultant complex gives rise to an alkyl-terminated polymer chain and a Ti−vinyl cation. Further polymerization at the Ti−vinyl center[69,70] would initially produce a vinyl-terminated chain. However, it has been demonstrated by Grubbs *et al.* that the vinyl chain end is likely to reinsert, giving rise to cyclized chain ends.[71]

(57) Species **22** was optimized by first constraining the Ti−C_{olefin}−C_{olefin} angle to 180°. This constraint was then relaxed in the final structure. Initial attempts to optimize an end-on olefin complex without the constraint lead to the π-complex.

species **24** and **27** are distinguished from one another by the orientation of the vinyl group relative to the coordinated ethane moiety. In **24**, the vinyl group is oriented toward the ethane moiety whereas in **27** it is oriented outward away from the coordinated ethane group. The free products arising from channel b, **28**, and ethane lie 20.3 kJ/mol below the free reactants.

Comparison of the two reaction channels a and b in Figure 2c shows that channel b is the preferred σ-bond metathesis channel. Complexation of the olefin strongly favors the formation of a π-complex as opposed to the end-on complex **22**. The end-on complex, **22**, not only is 30.3 kJ/mol less stable than the π-complex **10a** but also lies in a shallow well, allowing for facile isomerization to the π-complex. Although the barrier is 12.1 kJ/mol larger for channel b, the transition state itself lies 18.2 kJ/mol lower than the transition state for channel a.

To corroborate the result that channel b is favored, the transfer process was simulated with the CP-MD method. As with the other simulations, the growing chain was modeled with a propyl chain and the olefin modeled by an ethene monomer. A bidirectional scan was performed whereby a midplane reaction coordinate similar to that depicted in Figure 4 was utilized. The forward scan was initiated from a planar β-agostic π-complex(equivalent to **10b**) as opposed to the less stable end-on complex (equivalent to **22**). If the simulation was initiated from the end-on complex, the system would immediately revert to the π-complex since the π-complex is more stable. Nevertheless, the midplane reaction coordinate is flexible enough to allow for the end-on complex to form. The results of the reverse scan indeed confirm that this is the case, since no end-complex was observed.

Relevant geometric and energetic quantities plotted as a function of the slow growth reaction coordinate are displayed in Figure 10. The value of the reaction coordinate was varied from approximately -0.01 in the π-complex to 0.5, the value in the transition state region. The integrated force on the reaction coordinate which is plotted in Figure 10a shows that the free energy potential crests at a RC value of approximately 0.48. A snapshot(**29^{MD}**) of the system at this point is shown in Figure 11. When the Ti, C_1, and C_2 atoms are collinear, the olefin can be characterized as being coordinated to the metal in the end-on fashion (see Scheme 4 for atom labeling). The Ti$-C_2-C_1$ angle which is plotted as the shaded line in Figure 10b never dips below 60°, clearly indicating that the end-on olefin complex is not formed. Also plotted in Figure 10b is the Ti$-C_2-C_1-H_1$ torsion which distinguishes the π-coordination of the olefin from the edge-on coordination of the olefin as previously discussed. In the initial segment of the simulation this angle hovers around 90°, indicating π-coordination of the olefin. At a reaction coordinate value of 0.18, this dihedral angle gradually drops to a value near 0° at the end of the simulation. Thus, the edge-on coordination of the olefin is gradually adopted, showing that there is no formation of a stable edge-on olefin coordinated intermediate. Thus, the olefin σ-bond metathesis simulated by the CP-MD method corresponds to channel b of Scheme 4 and is in general agreement with the results of the static calculations of this channel.

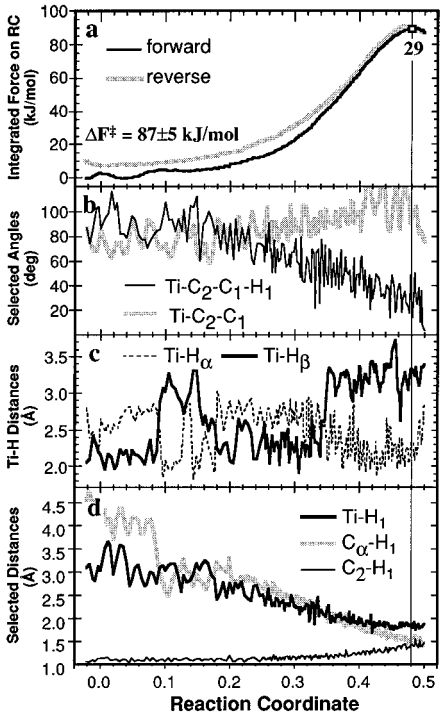

Figure 10. Selected structural and energetic quantities as a function of the reaction coordinate for Car-Parrinello MD simulation of the olefin σ-bond metathesis chain termination reaction:[40] (a) the integrated force on the reaction coordinate for the forward and reverse scans, (b) selected angles, (c): α- and β-agostic Ti$-$H bond distances, (d) selected distances. Scheme 4 depicts the atom labeling. The trajectories depicted in (b) and (c) correspond to the forward reaction only. The midplane constraint analogous to that defined in Figure 4 for the hydrogen transfer to the monomer simulation was used as the slow-growth reaction coordinate. The initial value of -0.01 approximates a β-agostic π-complex whereas the final value of 0.5 represents the transition state region. The vertical line represents the location of the snapshot structure **29^{MD}**.

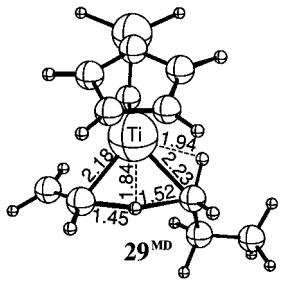

Figure 11. Snapshot structure from the transition state region of the Car-Parrinello molecular dynamics simulation of the olefin σ-bond metathesis process. The value of the midplane reaction coordinate in **29^{MD}** is 0.48.

Figure 10d traces the $C_\alpha-H_1$ and C_2-H_1 distances and shows that at the approximate transition state the $C_\alpha-H_1$ distance is roughly 1.5 Å, whereas the C_2-H_1 distance is slightly shorter. This asymmetry in the two C$-$H bonds agrees well with the transition state structure **26‡**. Both simulations indicate that the transferred hydrogen atom is somewhat closer to the olefinic carbon in the transition state. The Ti$-H_1$ distance which is also plotted in Figure 10d converges to a value of roughly 1.8 Å in the transition state, again in good agreement with the static calculations.

Plotted in Figure 10c are selected Ti−H_α and Ti−H_β bond distances. Following the two distances through the course of the simulation yields some interesting results. In the first segment of the simulation the β-agostic interaction is sustained until about a reaction coordinate value of 0.08 at which time a short lived α-agostic interaction forms. Although it is not shown in Figure 10, associated with the formation of the α-agostic bond is a rotation of the propyl group about the Ti−C_α bond. When the reaction coordinate reaches 0.18, the β-agostic interaction is reformed, with the β-methylene group of the propyl chain oriented toward the amido group. Thus, the initial planar β-agostic π-complex, akin to **10a**, isomerizes to the "rotated" β-agostic π-complex, similar to **10b**, passing through an α-agostic structure. As the transition state is approached the β-agostic interaction is again lost to the α-agostic interaction. Clearly there is α-agostic stabilization of the transition state where the Ti−H_α distance is approximately 2.2 Å. This is somewhat shorter than the 2.37 Å Ti−H_α distance in structure **26**‡.

Figure 10a traces the relative free energy of the olefin σ-bond metathesis process from the β-agostic complex to the transition state for both the forward and reverse scans. The Car-Parrinello MD simulation provides an estimate for the free energy barrier of $\Delta F^{\ddagger} = 87 \pm 5$ kJ/mol at 300 K. In good agreement with the MD simulation, the static simulation yields a free energy barrier at the same temperature of $\Delta F^{\ddagger} = 91.7$ kJ/mol.

Comparing the free energy barriers of the three termination processes examined—(1) β-hydrogen transfer to the monomer, (2) β-hydrogen transfer to the metal, and (3) olefin σ-bond metathesis—we find that hydrogen transfer to the monomer process is the most favored. This is dependent on the free energy barrier of olefin complexation to form the π-complex, which we have found to be barrierless.[6] We conclude that the primary termination process in Ti−CGC systems is the hydrogen transfer to the monomer. This process gives rise to vinyl-terminated chain ends, which then can potentially reinsert giving rise to long chain branching. We discuss this issue in the ensuing section.

3.b. Long Chain Branching. Constrained-geometry catalyst technology is claimed to produce polyethylenes which contain a substantial amount of linear long chain branches, and like other single-site catalysts they have narrow molecular weight distributions ($M_n/M_w \approx 2$).[2] This provides the polymers with the improved physical properties characteristic of metallocenes while at the same time making it possible to attain levels of processibility similar to those of low-density polyethylenes (LDPE).[3,58,59] The linear long chains are estimated to contain more than 250 carbon atoms[4] (to substantially effect the physical properties of the polymer) and occur at a frequency of 0.01−5 per 1000 carbon atoms with a preferable frequency of less than 1.[60] Scheme 6 depicts the generic structure of the linear long chain branched polymers that are proposed. The favored mechanism for long chain branch formation involves the reinsertion of polymer chains that contain a vinyl chain

Scheme 6

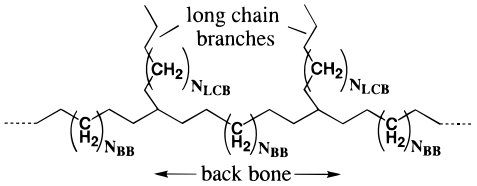

Scheme 7

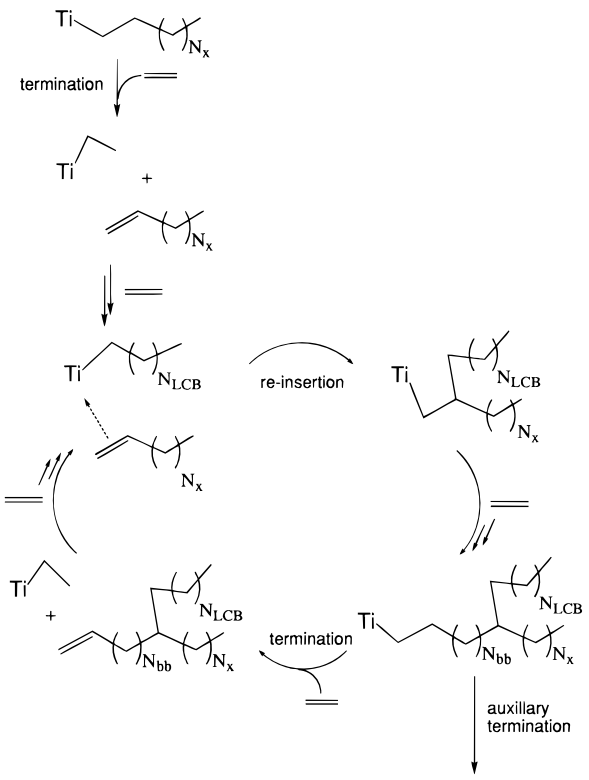

end, in particular those produced by chain termination via β-hydrogen transfer.[3] If these vinyl-terminated macromonomers can effectively compete with the monomer during insertion, long chains can be incorporated into the polymer as depicted in Scheme 7. The more open active site of the constrained-geometry catalysts suggests that it would be more accommodating in allowing a long chain to reinsert than the more sterically inhibited active site of the bis-Cp metallocene catalyst systems. We have examined aspects of the vinyl chain end reinsertion mechanism. In addition to this we have explored the feasibility of an alternative long chain branching mechanism through an alkyl σ-bond metathesis process which is illustrated in Scheme 9.

Reinsertion. Ti-based constrained geometry catalysts are claimed[2,61] to produce high molecular weight polymers with molecular weight distributions near the single-site theoretical limit[62] of $M_w/M_n \approx 2$. The high molecular weights are not in agreement with our calculated barriers for the insertion and termination processes. Our calculated difference in the free energy barriers of propagation[6] and chain termination is $\Delta\Delta F^{\ddagger}$ (ins-term) = 15.8 kJ/mol at 300 K which gives a chain length of approximately 1100 carbon atoms. This is in

(58) Knight, G. W.; Lai, S. *Proceedings of SPE Polyolefins VIII International Conference*, p 13, 1993.
(59) Swogger, K. W.; Kao, C. I. *Proceedings of SPE Polyolefins VIII International Conference*, p 13, 1993.
(60) Lai, S.; Wilson, J. R.; Knight, G. W.; Stevens, J. C. U.S. Patent No. 5278272, Jan. 11, 1994.
(61) Uozumi, T.; Toneri, T.; Soga, K. *211th American Chemical Society National Meeting*, New Orleans, LA, March 24−28.
(62) Flory, P. J. *Principles of Polymer Chemistry*; Cornell University Press: Ithaca, 1953.

stark contrast to experimental[63] molecular weights which are roughly in the order of 14 500 carbon atoms[64] at elevated temperatures (80 °C).

Outlined in Scheme 7 is a mechanism which can explain the observed high molecular weights which is consistent with our calculated $\Delta\Delta F^{\ddagger}$ (ins-term). Following activation of the precatalyst, chain propagation produces a Ti−alkyl complex as depicted at the top of Scheme 7. Chain termination via hydrogen transfer to monomer will result in a vinyl-terminated long chain branch of length N_x (in carbon units). The average length of this chain and therefore the average value of N_x is governed by $\Delta\Delta F^{\ddagger}$ (ins-term). Following the termination process, a new chain can grow at the active site. Now there is a competition between monomer insertion and the reinsertion of the previously terminated long chain. Since reinsertion of the macromonomer is much less favorable than ethene insertion due to steric effects and a significantly lower concentration, a chain segment of length N_{LCB} will be formed. (The LCB subscript is used because this chain segment will form what is considered to be a long chain branch.) Reinsertion of the macromonomer will produce a secondary carbon and therefore a branching point. Following reinsertion of the vinyl-terminated long chain, a new chain segment will be formed as monomer continues to insert. The length of the newest chain segment denoted by N_{BB} is again governed by the relative rate of insertion versus chain termination, $\Delta\Delta F^{\ddagger}$ (ins-term). Both N_{BB} and N_x are governed by the relative rate of insertion versus termination or $\Delta\Delta F^{\ddagger}$ (ins-term) and are related to one another by the following relationship $N_{LCB} + N_{BB} = N_x$. Repetition of this cycle depicted in Scheme 7 results in a linear long chain branched polymer whose structure is shown in Scheme 6. To reiterate, the length of the long chain branches (N_{LCB}) is governed by $\Delta\Delta F^{\ddagger}$ (ins-reins) and the length of the backbone segment plus the length of the long chain branch is determined by $\Delta\Delta F^{\ddagger}$ (ins-term).

Applying the above mechanism for the long chain branching to our calculated relative free energy barriers provide reasonable agreement with experimentally observed long chain branching frequencies and molecular weights. On the basis of our calculated $\Delta\Delta F^{\ddagger}$ (ins-term) at 300 K of 15.8 kJ/mol, we estimate $N_x = N_{BB} + N_{LCB}$ to be roughly 1100 carbon units. ^{13}C NMR experiments estimate the frequency of long chain branches to be in the range of 0.01−3 for every 1000 carbon atoms of the polymer.[65,66] A frequency of 1 long chain branch for every 1000 carbon atoms equates to a $N_x = N_{BB} + N_{LCB}$ value of 1000 carbon atoms. Thus, our results do fall in the range of long chain branching frequency determined experimentally.[67] Since we have not modeled the macromonomer reinsertion, we cannot provide an estimate for the length of the long chain branch segments, N_{LCB}. However, the rate of macromonomer reinsertion will greatly depend on the polymerization process.[4] For example, in slurry or gas phase processes the rate of macromonomer reinsertion is likely limited by the rate at which the macromonomer can diffuse through the polymer encapsulated active site.[4]

Scheme 8

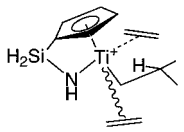

The high molecular weights and low polydispersities that are observed suggest that there is a secondary process which halts the reinsertion cycle (Scheme 7) and ultimately terminates the chain. This process may be a diffusive mechanism whereby the vinyl-terminated chain can no longer "reach" the active site or it may be a secondary termination process. If it is the latter, the overall chain length and therefore the molecular weight would be governed by the relative rate of monomer insertion compared the rate of the secondary termination process or $\Delta\Delta F^{\ddagger}$ (ins-2nd term). Our calculations suggest the most probable secondary termination process is β-hydrogen transfer to the metal which has a calculated free energy barrier of 54 kJ/mol at 300 K. We have found through molecular dynamics simulations that once the olefin−hydride complex establishes itself, the formation of a Ti−allyl−dihydrogen complex is thermodynamically barrierless.[52] Such a Ti−allyl complex could potentially terminate the reinsertion cycle. The $\Delta\Delta F^{\ddagger}$ (ins-2nd term) is 29.6 kJ/mol at 300 K. This gives a high molecular weight of 4×10^6 g/mol at 300 K or approximately 6.3×10^5 g/mol at 80 °C.[64] Although the molecular weight is overestimated, this mechanism can account for the observed linear long chain branching, narrow molecular weight distributions, and high molecular weights in CGC-based polymers.

The above reinsertion mechanism suggests that the long chain branch inserts back into the catalyst center in which it was originally formed. This further suggests that the vinyl-terminated long chain branch may be complexed to the catalyst center while the N_{LCB} segment is grown. To address this consideration, we have optimized several Ti−ethyl$^+$ olefin π-complexes which have a second monomer in the active site, as represented in Scheme 8. Several conformations were examined, all showing that the binding of the auxiliary olefin is negligible (under $\Delta H_{el} = 15$ kJ/mol). This is also consistent with our molecular dynamics simulations which show that even the primary olefin is likely to rapidly exchange with other monomer molecules.[6,34] Although we find no strong electronic complexation of an auxiliary olefin, the vinyl-terminated long chain branch may still be held in the coordination sphere of the catalyst center by other means. Here the cocatalyst may play a role, or the chain may simply be held by mechanical entanglement.[4]

Alkyl σ-Bond Metathesis. An alternative long chain branching mechanism is one which involves the transfer of a hydrogen atom from a "free" polymer chain to the α-carbon of the Ti−alkyl cation in a σ-bond metathesis process. This process is sketched in Scheme 9, where P_1 and P_2 represent two segments of the same polymer chain separated by a methylene group (labeled

(63) Canich, J. A. M. U.S. Patent No. 5096867, March 17, 1992.
(64) For homopolymerization of ethylene at 80 °C with $MePhSi(C_5Me_4)(N\text{-}t\text{-}Bu)TiCl_2$, ref 63 reported polyethylene molecular weights of 279 700 and 406 100 and for homopolymerization of ethylene at 80 °C with $Me_2Si(C_5Me_4)(NC_6H_4\text{-}p\text{-}OMe)TiCl_2$ the same patent reported a molecular weight of 529 100. This is an average molecular weight of 404 967 or 14 500 C units.
(65) Lai, S.; Wilson, J. R.; Knight, G. W.; Stevens, J. C.; Chum, P.-W. U.S. Patent No. 5272236, Dec 21, 1993.
(66) Lai, S.; Wilson, J. R.; Knight, G. W.; Stevens, J. C. International Patent Application WO 93/08221, April 29, 1993.
(67) The most preferrable rate of long chain branching as specified in ref 5 is 1−2 long chain branches per 1000 C.

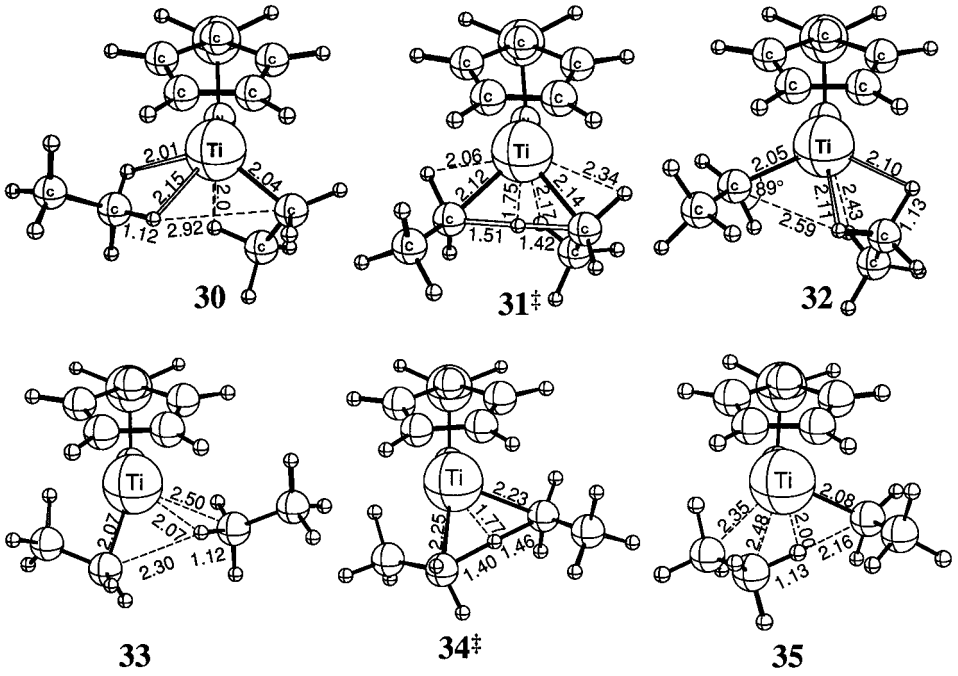

Figure 12. Optimized structures corresponding to the alkyl σ-bond metathesis process depicted in Scheme 9. Structures **30**, **31**‡, and **32** refer to reaction channel a whereas structures **33**, **34**‡, and **35** relate to channel b.

Scheme 9

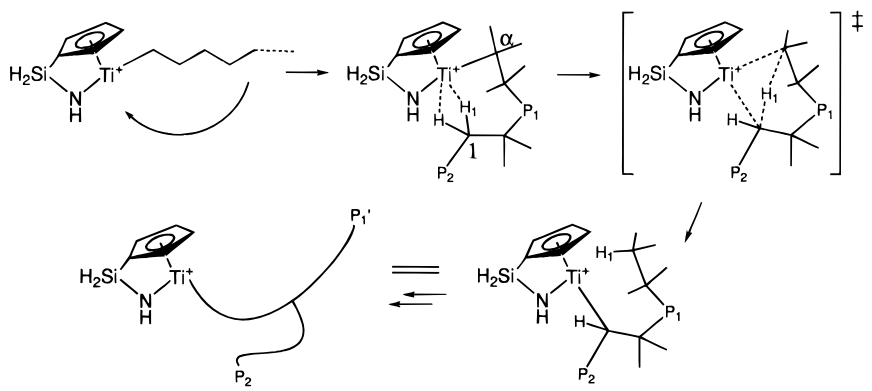

1). An adduct is proposed to initially form whereby the polymer forms agostic bonds with the metal center. This is followed by the transfer of a hydrogen atom (H_1) of the coordinated polymer to the α-carbon of the growing chain through a four-centered transition state. This chain transfer process followed by further monomer insertion would result in a long chain branching. This mechanism can be likened to the chain transfer processes responsible for branching in high temperature, high pressure free-radical processes which produce LDPE. Although this mechanism will lead to dendritic branching if it occurs at high frequency, at low frequencies it can produce linear long chain branching. Although Scheme 9 depicts a process where the growing polymer chain comes back and "attacks" itself, this is not necessarily the case. The chain segments P_1 and P_2 can also reside on a separate chains, originating from different active sites. Both scenarios will give rise to branching.

We have explored this process with both static and dynamics simulations. Sketched in Figure 12 are the stationary points that have been optimized for two distinct reaction channels, a frontside channel and a backside channel. For the static simulations, an ethyl group was used to model the growing chain, and an ethane moiety was used as a model for the incoming polymer chain that "bites back". Thus, in this simulation the chain segments P_1 and P_2 described in scheme 9 are modeled by CH_3 and H. It is assumed that the transferred hydrogen atom, H_1, must lie along the coordination plane of the CGC as observed with the other H transfer processes examined in this study. This requirement orients the chain segments P_1 and P_2 perpendicular to this plane, thereby directing one segment toward the Cp ring and the other segment toward the amido ligand of the CGC. In our static simulation we have oriented the CH_3 group toward the more sterically demanding Cp ring and the H atom toward the amido group.

The calculated reaction profiles for the frontside (solid) and backside (shaded) channels are illustrated in Figure 13. In both channels, the complexation of the ethane molecule to the Ti−alkyl cation is exothermic. The frontside adduct, **30**, lies 53.3 kJ/mol below the free Ti−alkyl cation and ethane molecule, while the backside adduct, **33**, is somewhat less stable, lying 44.7 kJ/mol below the baseline. Although we have not explored the complexation process, we expect there to be no steric or electronic barrier for our model system (although there may be a steric barrier associated with the complexation

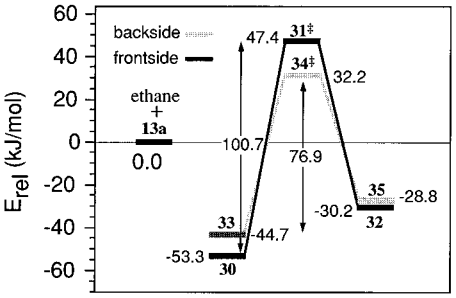

Figure 13. Calculated "static" energy profiles for alkyl σ-bond metathesis process (sp^3 C−H activation)—a potential long chain branching mechanism (Scheme 9). Two channels are explored.

for the real system due to the size of the incoming polymer chain). Although the general structure of the four-membered ring in the transitions states for the frontside, **31**‡, and backside, **34**‡, channels are similar, the barrier for the frontside channel is significantly larger than its backside counterpart. The frontside channel possesses an electronic barrier of 100.7 kJ/mol whereas the backside channel has a barrier of 76.9 kJ/mol. Complete transfer of the hydrogen atom from the polymer chain to the α-carbon of the Ti−alkyl complex forms a terminal adduct complex (**32** and **35**) which lies roughly 30 kJ/mol below the baseline for both the frontside and backside channels. Although the adducts **32** and **35** are equivalent to the incipient adducts **31** and **33**, the terminal adducts are slightly destabilized due to the orientation of the ethyl group toward the Cp rings.

The Car-Parrinello MD simulations of the alkyl σ-bond metathesis process substantiate the results of the static calculations.[68] In these simulations the growing chain was modeled by a propyl group and the incoming polymer was modeled by an ethane molecule. The slow-growth method was employed, and a midplane reaction coordinate was utilized as described in Figure 4. The slow-growth parameter was varied between an initial value typical of the Ti−alkyl cation−polymer adduct to a value of approximately 0.5, which approximates the transition state region. For the frontside channel, only a forward scan from the adduct to the transition state has been performed since the reverse scan reverted to the backside channel. This unidirectional scan resulted in an estimated free energy barrier of $\Delta F^{\ddagger}$(R = propyl) = 94 kJ/mol at 300 K, in reasonable agreement with the static electronic barrier of $\Delta H^{\ddagger}_{el}$(R = ethyl) = 100.7 kJ/mol. For the backside channel both forward and reverse scans have been performed and will now be discussed in detail.

Figure 14 follows relevant energetic and geometric parameters as a function of the slow-growth reaction coordinate for the backside reaction channel. As depicted in Figure 14a the free energy barrier for the backside channel as predicted by the Car-Parrinello simulation is $\Delta F^{\ddagger} = 70 \pm 3$ at 300 K. Again, the Car-Parrinello free energy barrier is in excellent agreement

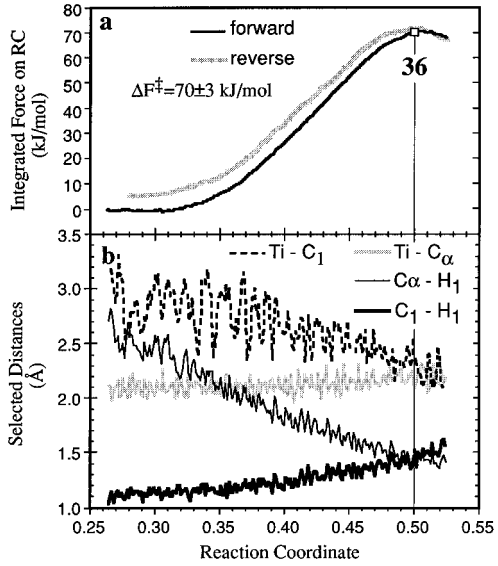

Figure 14. Selected structural and energetic quantities traced as a function of the reaction coordinate for Car-Parrinello MD simulation of the alkyl σ-bond metathesis chain termination reaction.[40] (a) The integrated force on the reaction coordinate for the forward and reverse scans. (b) Selected distances for the forward scan. Scheme 9 defines the atom labeling. The midplane constraint similar to that defined in Figure 4 was utilized as the slow growth reaction coordinate. The initial value of 0.26 corresponds to an ethane−Ti−propyl adduct similar to **33** whereas the value of 0.5 represents the transition state region. The vertical line represents the location of the snapshot structure **36**^{MD} (Figure 15).

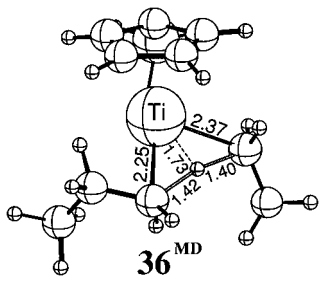

Figure 15. Snapshot structure from the transition state region of the Car-Parrinello molecular dynamics simulation of the alkyl σ-bond metathesis process. The value of the midplane reaction coordinate in **36**^{MD} is 0.50.

with the static free energy barrier of $\Delta F^{\ddagger} = 72.3$ kJ/mol at 300 K. Figure 14b displays the progression of various distances as the transition state is formed. The C_α−H_1 and C_1−H_1 distances (see Scheme 9 for atom labeling) converge to a value of approximately 1.45 Å at the transition state region, which agrees well with the static structure **34**‡. Both the Ti−C_α and Ti−C_1 distances in the transition state region are also in reasonable agreement with the transition state structure **34**‡. Shown in Figure 15 is a snapshot structure taken at the transition state region of the Car-Parrinello simulation of the backside channel. Although structure **36**^{MD} is an arbitrary snapshot structure taken from the MD simulation with a midplane value of 0.5, the general similarity between **34**‡ and **36**^{MD} is noticeable.

The free energy barrier for the alkyl σ-bond metathesis process is approximately 70 kJ/mol. This is too high to account for the frequency of long chain branching predicted by ^{13}C NMR in CGC homopolymers, even at

(68) In actuality it was through the CP-MD simulations that the backside alkyl σ-bond metathesis channel was discovered.

(69) Eisch, J. J.; Piotrowski, A. M.; Brownstein, S. K.; Gabe, E. J.; Lee, F. L. *J. Am. Chem. Soc.* **1985**, *107*, 7219.

(70) Hlatky, G. G.; Turner, H. W.; Eckman, R. R. *J. Am. Chem. Soc.* **1989**, *111*, 2728.

(71) Clawson, L.; Soto, J.; Buchwald, S. L.; Steigerwald, M. L.; Grubbs, R. H. *J. Am. Chem. Soc.* **1985**, *107*, 3377.

Table 1. Comparison of Static and Dynamic Free Energy Barriers

process	free energy barrier $\Delta F^{\ddagger}$ (kJ/mol) at 300 K: Car-Parrinello simulation[a,b]	static[d]	static with quantum effects[d]	$\Delta H^{\ddagger}_{el}$ (kJ/mol)	$\Delta H^{\ddagger}_{vib}$ (kJ/mol)	$\Delta S^{\ddagger}_{total}$ (J/mol·K)	ΔZPE (kJ/mol)
hydrogen transfer to monomer (Scheme 2)[e]	43 ± 8	43.0	40.1	31.7	1.7	−37.7	−4.6
hydrogen transfer to metal (Scheme 3)[f]	57 ± 3	65.4	53.9	66.8	0.5	+4.6	−12.0
olefin σ-bond metathesis (Scheme 4b)[e]	87 ± 5	93.8	91.7	92.6	−1.4	−4.1	−0.75
alkyl σ-bond metathesis (Scheme 9): backside channel[e]	70 ± 3	81.2	72.3	76.9	−2.1	−14.1	−6.8

[a] Does not include any quantum dynamical corrections such as zero point energy correction. Additionally, since the classical vibrational energy levels are continuous, $H_{vib} = \sum RT/2$ and $\Delta H_{vib} = 0$ for the MD simulations. [b] Reported values are the average of the forward and reverse scans. The reported error bars are half the difference between the forward and reverse scans. [c] Does not include zero-point energy correction and ΔH_{vib} to more correctly compare with Car-Parrinello MD free energies ($\Delta F = \Delta H_{el} - T\Delta S_{total}$). [d] Includes zero-point energy correction and ΔH_{vib} ($\Delta F = \Delta H_{el} + \Delta H_{vib} + \Delta ZPE - T\Delta S_{total}$). Does not include quantum tunneling. [e] An ethyl group is used to model the growing chain in the static simulation whereas a propyl group is used to model the growing chain in the molecular dynamics simulation. [f] A propyl group is used to model the growing chain in both static and dynamic simulations.

elevated temperatures. Our calculations therefore suggest that the most probable long chain branching mechanism is the reinsertion of vinyl-terminated chains. Concurrent occurrence of the alkyl σ-bond metathesis process would not influence the long chain branched characteristics of the polymer. However, an alkyl σ-bond metathesis process involving two different chains could give rise to complete termination.

4. Assessment of Computational Methods

Since the determination of free energy barriers at the *ab initio* level by molecular dynamics is somewhat novel, we briefly comment on the dynamic and static results. Table 1 compares the free energy barriers of the static calculations to those obtained by the Car-Parrinello simulations. Although there are important differences in the two simulations (most notably the model for the growing chain[72]), the static and dynamic free energy barriers are in remarkable agreement with on another. The mean absolute deviation between dynamically and "statically" (i.e. from the partition function of a harmonic oscillator) derived $\Delta F^{\ddagger}$ values is 3.3 kJ/mol (signed mean: −0.3 kJ/mol) and 8.8 kJ/mol (signed mean: −8.8 kJ/mol) if one corrects for the terms not present in the molecular dynamics simulations.

These results clearly demonstrate that the molecular dynamics simulations both complement and further corroborate the results of the static calculations well. The Car-Parrinello molecular dynamics method provides a general method of calculating accurate free energy barriers that are in excellent agreement with established static methods. Moreover, the molecular dynamics simulations provide an efficient manner to explore important regions of conformation space particularly for processes that have many potential reaction channels. We reiterate here that the Car-Parrinello simulations do not include any quantum dynamical effects. However, it is apparent from Table 1 that the relative vibrational enthalpies and zero-point energies are a minor factor in the reactions studied. Finally we point out that both static and dynamic methods do not account for quantum tunneling effects.

(72) The reason for this discrepancy was our intent to use the largest, most realistic model for the growing chain that we could computationally afford. At the time, this was an ethyl chain for the static calculations and a propyl chain for the molecular dynamics calculations. Since the time the static calculations were initiated, we have improved the efficiency of our static (ADF) code by over a factor of 2.

5. Conclusions

We have examined chain termination and long chain branching processes for the constrained-geometry olefin polymerization catalyst ($CpSiH_2NH$)Ti-R^+. Both conventional static electronic structure calculations and Car-Parrinello molecular dynamics simulations at the nonlocal density functional level have been performed. Three distinct chain termination processes have been studied: (i) β-hydrogen transfer to the monomer, (ii) β-hydrogen transfer to the metal, and (iii) olefin σ-bond metathesis. The electronic barriers ($\Delta H^{\ddagger}_{el}$) and free energy barriers ($\Delta F^{\ddagger}$) found for the three processes are (i) $\Delta H^{\ddagger}_{el}$(R = ethyl) = 32 kJ/mol; $\Delta F^{\ddagger}$(R = ethyl) = 40.1; $\Delta F^{\ddagger}$(R = propyl) = 43 ± 8 kJ/mol at 300 K, (ii) $\Delta H^{\ddagger}_{el}$(R = ethyl) = 107 kJ/mol; $\Delta H^{\ddagger}_{el}$(R = propyl)= 67; $\Delta F^{\ddagger}$(R = propyl)= 57 ± 3 kJ/mol at 300 K, and (iii) $\Delta H^{\ddagger}_{el}$(R = ethyl) = 93; $\Delta F^{\ddagger}$(R = ethyl) = 91.7; $\Delta F^{\ddagger}$(R = propyl) = 87 ± 5 kJ/mol at 300 K. We conclude that the primary chain termination process is (i) hydrogen transfer to the monomer. We have also examined two long chain branching mechanisms (i) the conventional vinyl chain end reinsertion mechanism and (ii) an alternative alkyl σ-bond metathesis mechanism. Our calculated barrier for the alkyl σ-bond metathesis process is determined to be $\Delta H^{\ddagger}_{el}$(R = ethyl) = 76; $\Delta F^{\ddagger}$(R = ethyl) = 72.3; $\Delta F^{\ddagger}$(R = propyl) = 70 ± 3 at 300 K. Such a barrier is too high to account for the observed frequency of long chain branches. Our calculations therefore suggest that the most probable long chain branching mechanism is due to the reinsertion of vinyl-terminated chains. The calculated difference in the free energy barriers of insertion versus chain termination by hydrogen transfer to monomer is too small to account for the observed molecular weights. We therefore propose that the overall chain length is determined by an auxiliary process, such as chain termination by hydrogen transfer to the metal followed by allyl formation (Scheme 5) or alkyl σ-bond metathesis.

As noted in the first part of this study,[6] we have neglected the solvent and the counterion, both of which may play a role in the chemistry of the catalyst system. In a similar manner, we have also neglected the potential importance of the bulky alkyl substituents which are generally situated on the amido ligand. It should be further noted that the long chain branching technologies patented by DOW and EXXON are as much process technologies as they are catalyst technologies.

Finally we have demonstrated the utility and generality of using "first-principles" molecular dynamics

simulations to calculate free energy barriers for chemical reactions. The free energy barriers for the aforementioned processes were calculated by both conventional static calculations and by Car-Parrinello molecular dynamics. The results were in remarkable agreement with one another.

Acknowledgment. This investigation was supported by the Natural Science and Engineering Research Council of Canada (NSERC), as well as by the donors of the Petroleum Research Fund, administered by the American Chemical Society (ACS-PRF No 31205-AC3). The authors are greatly indebted to the staff of Novacor Research and Technology (Calgary) for the interesting discussions, particularly Dr. L. Fan, Dr. D. Harrison, and Dr. J. McMeeking. We thank Dr. L. Resconi for sending us preprints of his work, and we thank Prof. W. Piers for his discussions. P.M.M. would like to thank the Austrian Fonds zur Förderung der wissenchaftlichen Forschung (FWF) for financial support within project JO1099-CHE. T.K.W. wishes to thank NSERC, the Alberta Heritage Scholarship Fund, and the Izaak Walton Killam memorial foundation for financial support.

OM970126D